

Image transmission through an optical fiber using real-time modal phase restoration

Alexander Fertman and Dvir Yelin*

Department of Biomedical Engineering, Technion—Israel Institute of Technology, Haifa 32000, Israel

**Corresponding author: yelin@bm.technion.ac.il*

Received July 23, 2012; revised November 13, 2012; accepted November 18, 2012;
posted November 19, 2012 (Doc. ID 173087); published December 13, 2012

Theoretical analysis of a method for transmitting a complex image field through a single multimode optical fiber is presented. Using a known reference image, we show that it would be possible to evaluate the instantaneous modal dispersion of the fiber and use the knowledge of accumulated modal phases to recover the object field. For measuring the complex object and reference fields emanating from the fiber, we propose using a simple arrangement of two cameras for recording the intensity and Fourier images, followed by a modified Gerchberg–Saxton algorithm for full complex field reconstruction. While some experimental challenges could still be expected in any future implementation of this approach, we believe it would eventually allow the first image transmission through a long, multimode optical fiber. © 2012 Optical Society of America

OCIS codes: 100.3020, 100.5070, 110.2350, 260.2030.

1. INTRODUCTION

Transmitting an image through a single optical fiber is an important challenge in various fields that call for efficient visual data transfer across long distances, through narrow passages, or from hard-to-reach areas. While current fiber optic technology offers excellent light transmission at a wide range of wavelengths, phase distortions during light propagation prevent a single, large-core fiber from preserving image details. Currently, practical methods for image transfer by fiber optics were developed primarily for clinical diagnosis applications, including bundles comprising thousands of fibers, distal mechanical scanning of the light emanating from a single fiber [1,2], or spectral encoding techniques [3–5]. All these technologies, however, require sophisticated probe design and costly manufacturing procedures (i.e., fiber bundle assembly, scanning mechanism alignment, miniature optics fabrication, etc.).

The biggest obstacle for successful transmission of an image through a large-core multimode fiber is its modal dispersion; it has been shown that image scrambling occurs over very short distances even in ideal straight fibers [6]. One approach for overcoming the modal phase problem is by employing phase conjugation techniques between two successive transmissions through the same fiber [7] or through two identical fibers [8,9]. While this approach is capable of transmitting relatively high-quality images in real time, it would be unsuitable for applications that require image transmission from one end of the fiber to another due to the difficulty to manufacture and position two long, identical (and motionless) fibers. A method for transmitting an image from one end of a fiber to another has been proposed and theoretically studied [10] using interference between an image and reference fields on a nonlinear photorefractive crystal, potentially enabling real-time compensation of modal dispersion using phase conjugation through four-wave mixing. Recently, image transmission through a standard multimode stationary fiber was demonstrated [11,12] by utilizing digital holography

techniques and a calibration procedure that establishes the transformation matrix between orthogonal modes.

In this paper, we propose and theoretically analyze a technique for transmitting an image between two opposite ends of a single multimode optical fiber that does not require phase conjugation or the use of any nonlinear optical processes. Our approach is based on the transmission of a reference image in addition to the object image, which would serve for computing the instantaneous modal dispersion and applying the results for recovering the unknown, scrambled image. Because the two (image and reference) fields could be transmitted and captured almost simultaneously, this technique could allow image transfer across long fibers with little sensitivity to fiber motion. Moreover, the use of straightforward linear detection methods, which do not require the use of nonlinear crystals, would potentially allow the transmission of weak fields, minimizing undesired nonlinear effects within the fiber and allowing the use of simple light sources and detectors.

2. MATHEMATICAL MODEL

Our approach for image transmission through a single optical fiber is schematically illustrated in Fig. 1(a) and outlined in a flow chart in Fig. 1(b). First, a reference field ($E_{\text{ref.in}}$) is coupled into the multimode fiber; its complex output emanating from the other end of the fiber, denoted by $E_{\text{ref.out}}$, is measured; and the accumulated relative phase $\Delta\phi$ of the different propagation modes is calculated. Next, the object field, denoted by E_{in} , is coupled into the fiber and its complex output field E_{out} is measured. Assuming that fiber parameters remained constant between the transmissions of the object and reference fields, the calculated set of accumulated modal phases is now used for numerically compensating for the modal phases of the output object field, thus recovering the original input field E_{in} .

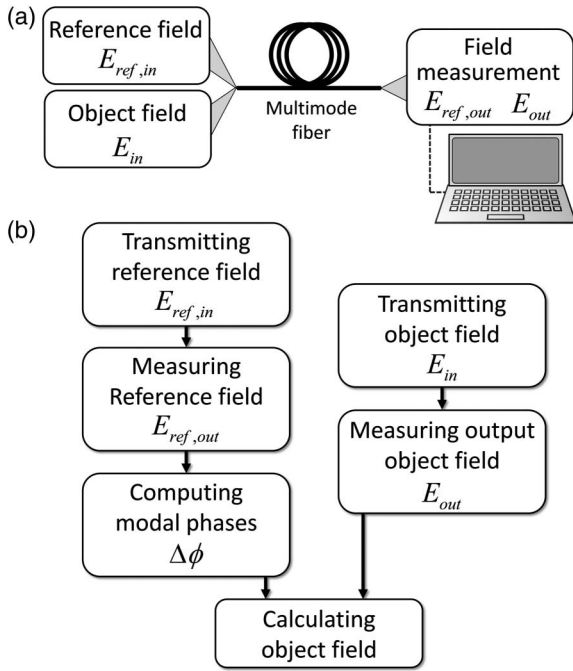


Fig. 1. (a) Schematic of the method for transmitting an image through a single optical fiber. (b) Flow chart outlining the various steps for computing the accumulated modal phases and recovering the object image.

Our mathematical model assumes an ideal, weakly guiding step-index fiber having core and cladding refractive indices n_c and n_{cl} , respectively, which satisfy the inequality $(n_c^2 - n_{cl}^2)/2n_c^2 \ll 1$. The propagation of an electromagnetic field in such optical fiber could be conveniently simulated using the linearly polarized (LP) modes [13]—a set of orthogonal eigenmodes of the fiber that spans all propagating fields. Using cylindrical coordinates with the z axis parallel to the main fiber axis, the electric field of each LP mode polarized in the x axis is described by its azimuthal (l) and radial (m) mode numbers according to

$$E_x^{lm}(r, \theta, z) = \begin{cases} E_0^{lm} J_l(u_{lm} \frac{r}{r_c}) \cos(l\theta) \exp(-i\beta_{lm} z), & r \leq r_c \\ E_0^{lm} \frac{J_l(u_{lm})}{K_l(w_{lm})} K_l(w_{lm} \frac{r}{r_c}) \cos(l\theta) \exp(-i\beta_{lm} z), & r \geq r_c \end{cases}, \quad (1)$$

where E_0^{lm} is a normalization constant, J_l is the Bessel function of the first kind of order l , K_l is the modified Bessel function of the second kind of order l , r_c denotes the fiber core radius, u_{lm} and w_{lm} are the normalized transverse phase and attenuation constants, respectively, and the propagation constant β_{lm} of each mode is given by

$$\beta_{lm} = \beta(u_{lm}, r_c) = \sqrt{k_0^2 n_c^2 - \frac{u_{lm}^2}{r_c^2}}, \quad (2)$$

where $k_0 = 2\pi/\lambda$ and λ denotes the optical wavelength. In addition to these modes, each mode with $l \neq 0$ has also a twin mode with an orthogonal helical polarity, mathematically expressed by replacing the cosine in Eq. (1) with a sine term. For the full representation of the optical field one needs also to consider the orthogonal polarization modes $E_y^{lm}(r, \theta, z)$; we will be omitting these modes from our simulations for brevity, that is, $E^{lm} = E_x^{lm}$, and we will discuss the effect of polarization diversity in the discussion section below.

In order to simulate image coupling into a multimode fiber, we assume that the object is imaged onto the face of the fiber using an ideal optical relay system that demagnifies the object image and adjusts its spatial extent to the dimensions of the fiber core [Fig. 2(a)]. After the optical relay system, the object field could be expressed as a superposition of the LP modes according to

$$E_{in} = \sum_{l,m} a_{in}^{lm} E^{lm}, \quad (3)$$

where the summation is over all possible real ($E^{lm} = (E^{lm})^*$) propagation modes, and a_{in}^{lm} denotes the complex amplitude

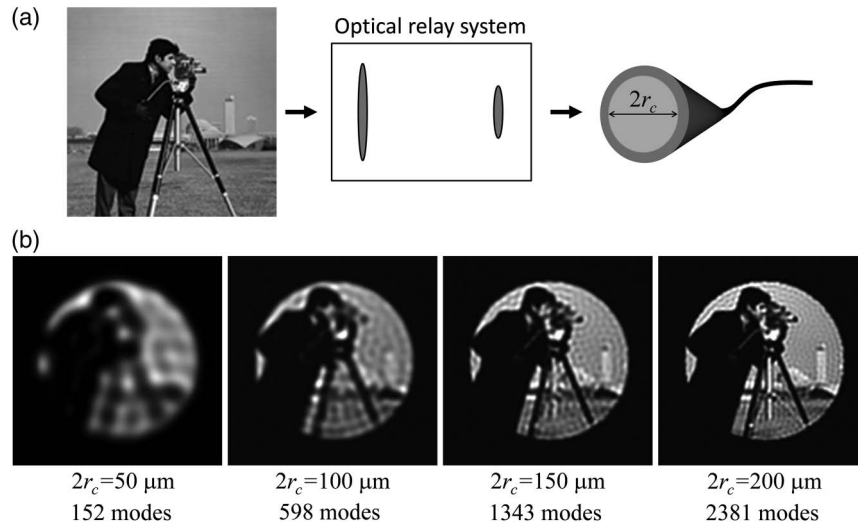


Fig. 2. (a) Input field coupling into a multimode fiber. (b) The resulting images expressed as superposition of LP modes of different core diameters ($2r_c$).

coefficient of each mode lm , calculated using the overlap integral

$$a_{in}^{lm} = \int_s E_{in} E^{lm} ds, \quad (4)$$

where s denotes the fiber cross-section area. Spanning the space of all possible propagation fields in a fiber, the total number of propagation modes N_m would determine the overall fidelity of the transmitted image: high-order modes contain high spatial frequencies and therefore allow the transmission of fine details in an image. The effect of the number of modes on image quality is evident by plotting the coupled field intensity $|E_{in}|^2$ of the image termed ‘‘Cameraman’’ into 50, 100, 150, and 200 μm diameter fibers, supporting up to 152, 598, 1343, and 2381 LP modes, respectively [Fig. 2(b)]. Refractive indices of the core and the clad were assumed to be 1.4570 and 1.4537, respectively, and the wavelength was 632.8 nm. For quantifying the improvement in image quality, the point-spread function (PSF) was calculated by simulating the coupling of a point image into the fiber. The total number of resolvable points N_p was then evaluated by dividing the total fiber cross section by the effective area of a hexagon whose apothem a equals half the width at e^{-1} of the maximum of the PSF:

$$N_p \cong \frac{\pi}{8\sqrt{3}} \frac{(2r_c)^2}{a^2}. \quad (5)$$

The number of resolvable points N_p (blue circles) and the number of propagation modes N_m (red squares) are plotted in Fig. 3 for different core diameters between 10 and 200 μm , showing nearly identical dependence on the normalized frequency parameter V of the fiber. The well-known approximation for the number of modes in a large-core fiber $N_m = V^2/4$ (single polarization) is plotted by a dashed curve for reference.

After coupling into the fiber, field propagation could be simulated by multiplying the complex amplitude of each mode a_{in}^{lm} by a complex coefficient b^{lm} , which indicates its attenuation ($|b^{lm}| \leq 1$) and phase change ($\Delta\phi^{lm} = \text{angle}\{b^{lm}\}$) during

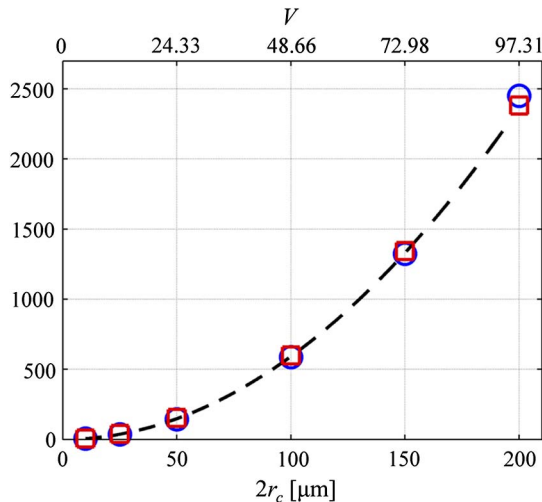


Fig. 3. (Color online) Number of resolvable points (blue circles) and number of propagation modes (red squares) as a function of the fiber’s core diameter and normalized frequency parameter. Dashed curve: $N_m = V^2/4$ (see text).

propagation. In many cases where fiber length is of the order of several meters, energy losses could be neglected; each mode maintains its power ($|b^{lm}| = 1$) but accumulates a different phase owing to its propagation constant β^{lm} : $\Delta\phi^{lm} = -\beta^{lm}z_0$, where z_0 denotes the total fiber length. Here, we also assume that the optical fiber is uniform along its main (z) axis and neglect strong fiber bends, essentially assuming no energy coupling between different modes. This assumption, of course, is clearly an idealization that would need to be validated experimentally in a future work. Under these assumptions, the field emerging from the fiber output is given by

$$E_{out} = \sum_{l,m} a_{in}^{lm} b^{lm}(z_0) E^{lm} = \sum_{l,m} a_{in}^{lm} e^{i\Delta\phi^{lm}(z_0)} E^{lm}, \quad (6)$$

and ideally could be calculated using the known input field and the modes’ propagation constants. The propagation of the input field generated from coupling the cameraman image (Fig. 4, top panel) through a 150 μm diameter fiber ($V = 72.985$) was simulated using Eq. (6) for different fiber lengths (Fig. 4, lower panels). Although the total image brightness was preserved during propagation, the accumulated phase differences between the various modes caused rapid image degradation [6]; after only 2 mm (Fig. 4, bottom right panel), details in the original input image were completely lost. Despite the rapid drop in image detail, the input object field could, in principle, be calculated (assuming an ideal, motionless fiber) from the output field E_{out} in a straightforward manner by first calculating its complex amplitude coefficients a_{out}^{lm} using

$$a_{out}^{lm} = \int_s E_{out} E^{lm} ds, \quad (7)$$

and then backpropagating the different modes by assigning an opposite set of modal phases $-\Delta\phi^{lm} = -(-\beta^{lm}z_0)$ to obtain the input object field:

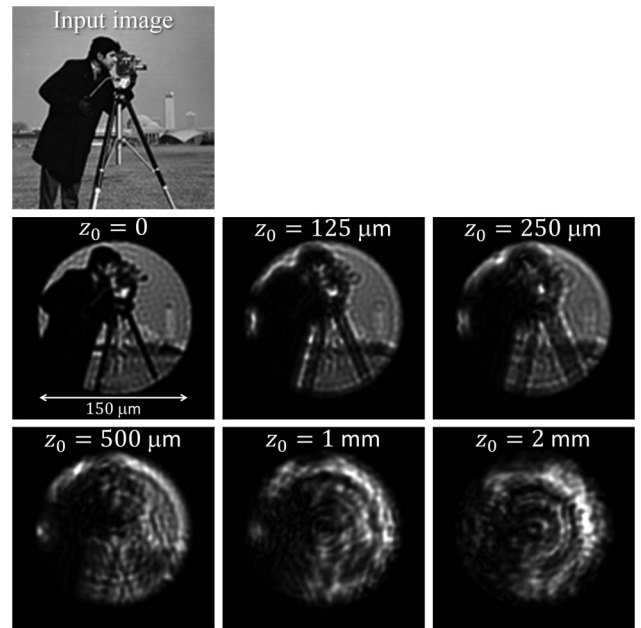


Fig. 4. Image propagation in 150 μm core diameter fiber ($V = 72.985$).

$$E_{\text{in}} = \sum_{l,m} a_{\text{out}}^{lm} e^{-i\Delta\phi_i} E^{lm}. \quad (8)$$

In reality, however, fiber imperfections even within the design tolerances, such as various defects, fiber bends, and local strains, would significantly affect the rate at which the phase of each mode is accumulated. Moreover, variations of fiber parameters caused, for example, by fiber motion, vibrations, and temperature changes would often prevent practical measurement or characterization of the phase accumulation. To account for such effects, we will be assuming that the accumulated modal phases cannot be calculated analytically and therefore must be considered *completely random* for any practical purpose, even after propagation through a few centimeters of a multimode fiber. Moreover, the random modal phases could not be assumed to remain constant over time and would be extremely sensitive to temporal fiber variations. Any measurement of the modal phases would thus need to be sufficiently fast to avoid detail washout, and the time gaps between successive measurements need to be short compared to the characteristic time scales of the modal dispersion changes.

3. REFERENCE IMAGE TRANSMISSION

In order to allow the calculation of the accumulated phase for each mode $\Delta\phi^{lm}$ at high signal-to-noise ratios, a reference field containing *all* LP modes with uniformly distributed amplitudes needs to be generated and transmitted through the fiber. An example for such a reference field ($a_{\text{in,ref}}^{lm} = 1$) is shown in Fig. 5(a), comprising two linear features extending from the core center to its circumference. The corresponding coefficients of the LP modes comprising this field are plotted in Fig. 5(b) using two-dimensional gray-scale representations of the amplitudes $|a_{\text{in,ref}}^{lm}|$ and phases $\text{angle}(a_{\text{in,ref}}^{lm})$ of each mode. The horizontal and vertical axes in Fig. 5(b) represent different values of l and m , respectively. Values on the right-(left-) hand side of $l = 0$ correspond to the coefficients that include the cosine (sine) modes. After coupling the reference image into the fiber, each mode then propagates and emerges from the fiber output, accumulating a total phase $\Delta\phi_{\text{ref}}^{lm}$, which could be calculated from the measured output coefficients [Eq. (7)] and from the known input coefficients [Fig. 5(b)] according to

$$\Delta\phi_{\text{ref}}^{lm} = \text{angle}(a_{\text{ref,out}}^{lm}) - \text{angle}(a_{\text{ref,in}}^{lm}), \quad (9)$$

where

$$a_{\text{ref,out}}^{lm} = \int_s E_{\text{ref,out}} E^{lm} ds, \quad (10)$$

$$a_{\text{ref,in}}^{lm} = \int_s E_{\text{ref,in}} E^{lm} ds = 1. \quad (11)$$

Assuming a linear optical system, the accumulated phases $\Delta\phi_{\text{ref}}^{lm}$ would depend only on the fiber properties and not on the field itself. Therefore, if fiber parameters are unchanged between the transmissions of the reference and object fields, we could assume that

$$\Delta\phi^{lm} = \Delta\phi_{\text{ref}}^{lm}, \quad (12)$$

that is, similar phases for all the modes comprising the object and the (known) reference fields. After calculating the reference phases, these phases can now be used for recovering the object field even for fibers much longer than the characteristic length at which modal dispersion dominates. Once $\Delta\phi_{\text{ref}}^{lm}$ (and therefore $\Delta\phi^{lm}$) is known for each mode, the transmitted object field could be calculated using Eq. (8).

4. MEASURING OUTPUT FIELDS

Unfortunately, conventional CCD and complementary metal-oxide-semiconductor (CMOS) cameras can only capture optical intensity and thus cannot directly measure complex fields; phase information of a field is often computed based on a number of intensity images. Various methods for recovering complex fields exist in the scientific literature, including the use of the Shack–Hartmann wavefront sensor [14], as well as newer methods for phase reconstruction using self-referencing [15], multiple-beam interferometry [16], and parallel-planes imaging [17], all of which could be utilized for measuring the complex output fields $E_{\text{ref,out}}$ and E_{out} emanating from the fiber. Our approach for measuring the output fields relies on capturing the intensities of the output field I_{out} and of its Fourier transform \tilde{I}_{out} [Fig. 6(a)], followed by the

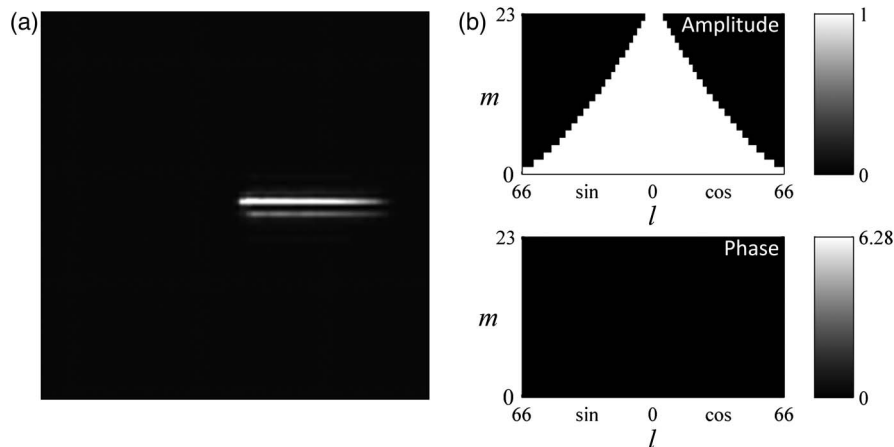


Fig. 5. Input reference field for calculating modal phase. (a) Intensity image. (b) Amplitudes (top) and phases (bottom) of the modes comprising the reference field.

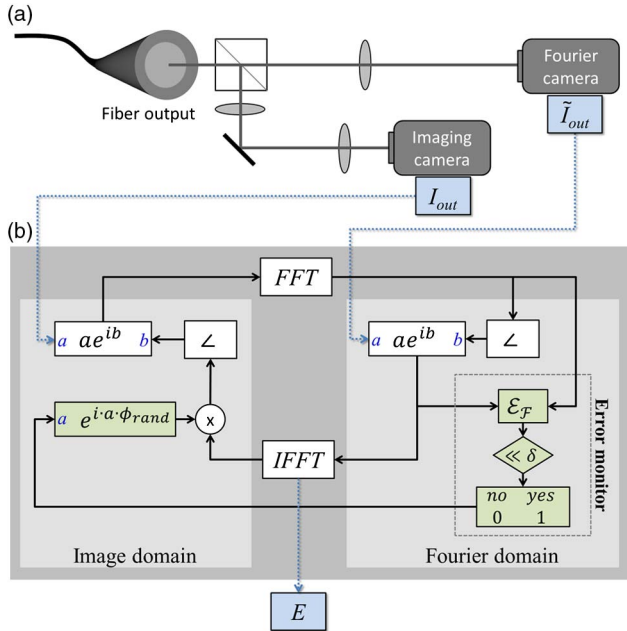


Fig. 6. (Color online) Extracting the complex output fields from two intensity images. (a) The output field is split into two imaging channels; one captures an intensity image, the other captures a Fourier image. (b) The captured images serve as the inputs to a modified Gerchberg–Saxton algorithm with a small-error monitor. FFT, fast Fourier transform; IFFT, inverse fast Fourier transform. \angle : angle.

recovery of the phases using a modified Gerchberg–Saxton [18] algorithm [Fig. 6(b)]. The proposed technique attempts to avoid the use of sophisticated optical components and could potentially allow high-resolution measurements with

a large dynamic range. Briefly, the Gerchberg–Saxton algorithm includes [Fig. 6(b)] iterative transformations between the object domain and its Fourier domain while forcing the measured amplitude constraints in both domains. We have found that without any modification, the Gerchberg–Saxton algorithm had a relatively low success rate of less than 75% for different simulated object fields due to occasional convergence to local minima.

In order to improve the success rate of the algorithm, we have added an error monitor at the Fourier domain [see Fig. 6(b)], which served to reduce convergence into local minima. After each iteration j , the error e^j was calculated using

$$e^j = \frac{1}{S} \int_S ||\text{FFT}\{E^j\}|^2 - \tilde{I}_{out}|^2 ds, \quad (13)$$

where E^j denotes the calculated field at iteration j and FFT denotes fast Fourier transform. Convergence of the algorithm was detected by comparing the error changes between successive iterations to a user-predefined threshold value. Error changes smaller than this value had initiated the addition of a random phase to each pixel in the image at gradually decreasing magnitudes. Assuming ideal conditions (no noise, accurate imaging), the addition of the error monitor has improved the success rate of the algorithm from approximately 75% to nearly 100%.

5. SIMULATION RESULTS

In order to test our approach for transmitting an image through a multimode fiber, a reference field [Fig. 7(a), see also

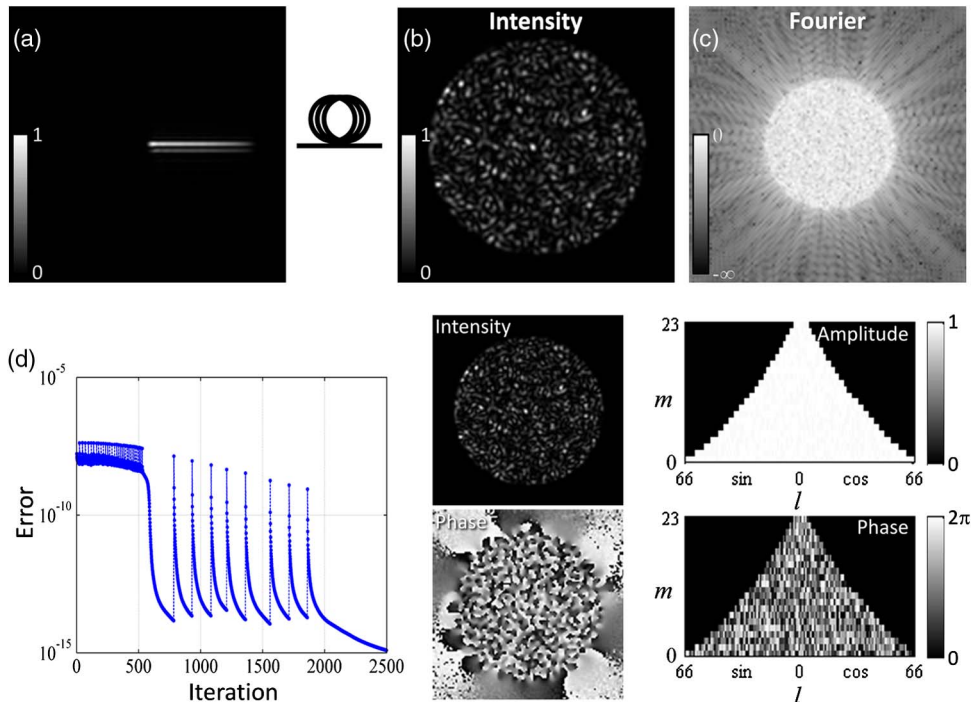


Fig. 7. (Color online) Reference field transmission, acquisition, and calculation of the complex mode coefficients. (a) Reference field intensity at the fiber input. (b) Intensity image recorded by the imaging camera. (c) Intensity image recorded by the Fourier camera (logarithmic scale). (d) Left: error parameter during algorithm convergence. Middle: resulting intensity (top) and phase (bottom) of the output field calculated by the Gerchberg–Saxton algorithm. Right: amplitudes (top) and phases (bottom) of the lm mode coefficients comprising the calculated output field.

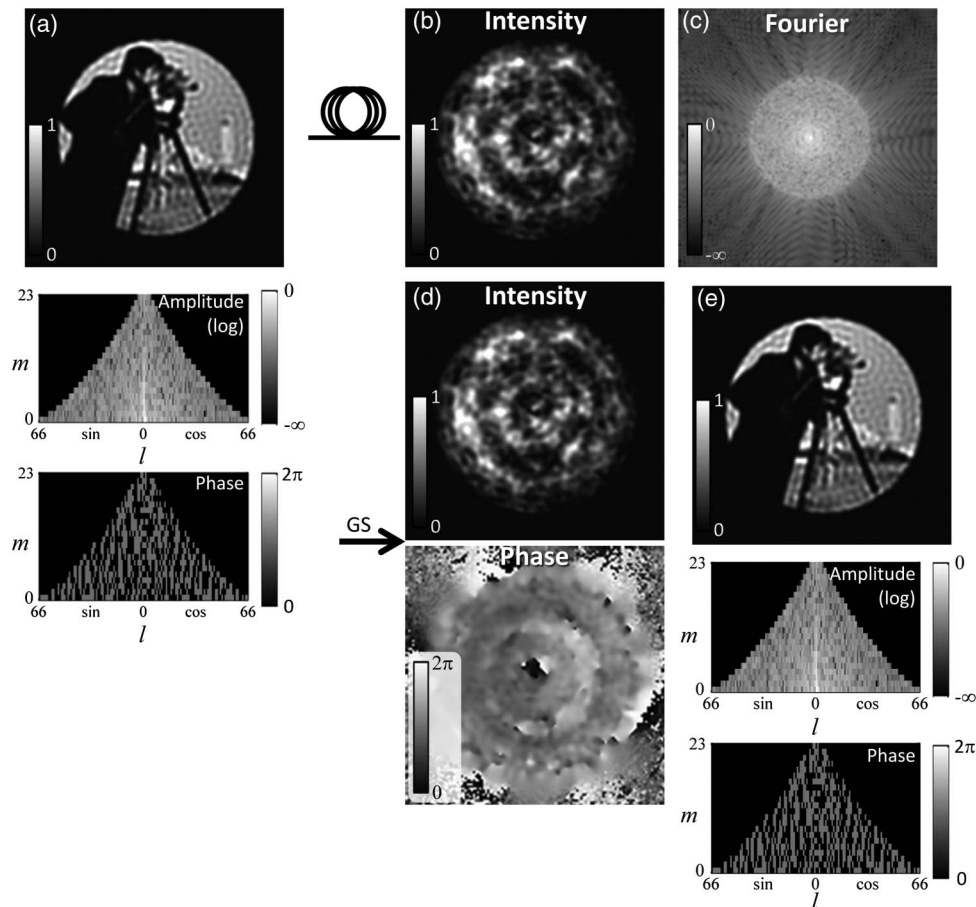


Fig. 8. Simulating image transmission and recovery. (a) Input image and its comprising mode coefficients. (b) Output image recorded by the imaging camera. (c) Output image recorded by the Fourier camera (logarithmic scale). (d) Intensity (top) and phase (bottom) of the output complex field calculated by the Gerchberg–Saxton algorithm. (e) Intensity and the mode coefficients of the recovered image, showing good correlation with the input image (a).

Fig. 5] was expressed as a superposition of the LP modes [Eq. (3)] of a $150\ \mu\text{m}$ diameter fiber core ($V = 72.985$). The reference field propagation across the entire (arbitrary) length of the fiber was simulated by assigning a random phase to each propagation mode. The measurement of the reference field emerging from the fiber output was simulated by computing the field intensity [I_{out} , Fig. 7(b)] and the intensity of its two-dimensional Fourier transform [\tilde{I}_{out} , Fig. 7(c)]. Using these two inputs, our modified Gerchberg–Saxton algorithm was applied to calculate the complex output field using 2500 iterations [Fig. 7(d), left panel], and the resulting output reference field [Fig. 7(d), middle panels] was then expressed as a superposition of the fiber's LP mode coefficients [Fig. 7(d), right panels]. Note the abrupt error rises during algorithm progression indicative of the addition of the random phases when error changes below the threshold value were detected. The resulting output field was obtained after approximately 15 s using MATLAB software, with 128×128 pixel images and full pixel depth (64 bit). The output field from the Gerchberg–Saxton algorithm showed close similarity to the actual simulated field both in amplitude [Fig. 7(b)] and phase (data not shown), verifying a successful convergence to a global minimum.

Next, after transmission of the reference image and the calculation of the accumulated modal phases [Fig. 7(d), bottom

right panel], we have simulated the transmission of the cameraman image [Fig. 2(a)] by assigning to its LP mode coefficients [Fig. 8(a)] the same random set of phases that was used to simulate the reference field propagation [Eq. (12)]. The output image [Fig. 8(b)] and its Fourier transform image [Fig. 8(c)] were then used by the modified Gerchberg–Saxton algorithm to compute the complex output field [Fig. 8(d)]. Finally, by expressing the output field in terms of its propagation modes using Eq. (7) and by subtracting the accumulated modal phases computed from the reference field, the input field of the cameraman was recovered [Fig. 8(e)], showing good resemblance to the input image with similar complex mode coefficients [Fig. 8(a)].

The presented method could recover not only the intensity of an input field but also its phases. It would thus be possible to transmit and recover full complex fields or phase-only images of transparent objects such as cells and biological tissue. To simulate the transmission of a phase image, we have numerically generated a phase field of a single cell [Fig. 9(a)] and simulated its transmission through a $150\ \mu\text{m}$ diameter fiber ($V = 72.985$) by assigning random modal phases to its modal coefficients. The output intensity [Fig. 9(b)] and Fourier [Fig. 9(c)] images were then used for calculating the output complex field, while the accumulated modal phases were calculated from reference image transmission

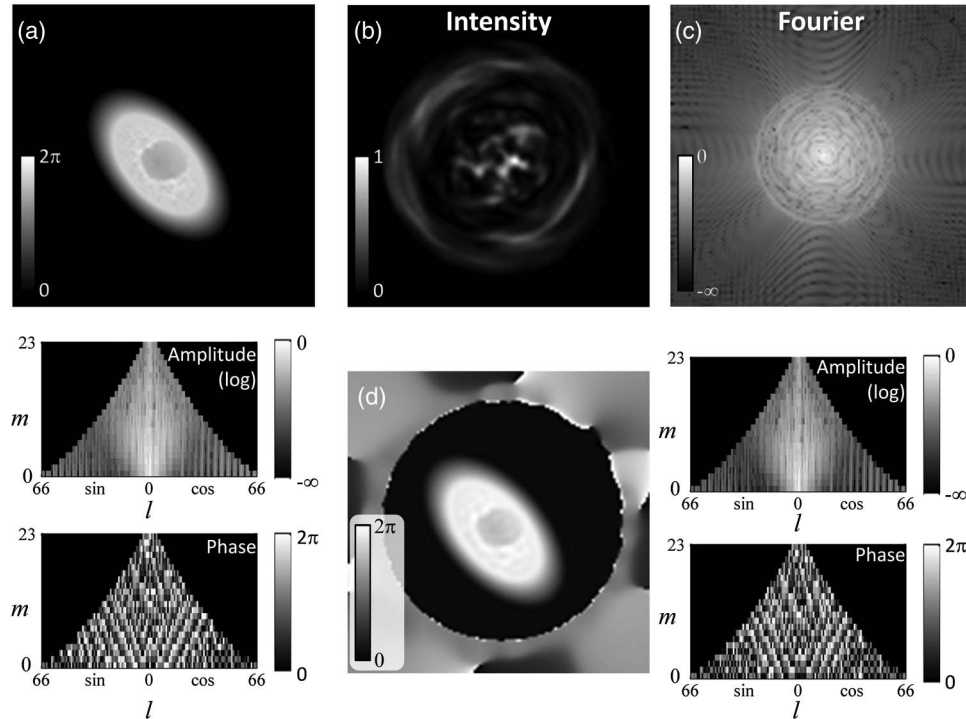


Fig. 9. Phase-only image transmission and recovery. (a) Object phase image (top) and its corresponding mode coefficients (bottom). (b) Intensity output image recorded by the imaging camera. (c) Intensity output image recorded by the Fourier camera (logarithmic scale). (d) Recovered phase image (left) and the corresponding mode coefficients (right) of the input field, showing good correlation with the input image (a).

(Fig. 5), which were subsequently used to recover the original phase image of the cell [Fig. 9(d)].

6. SENSITIVITY TO NOISE

In any practical implementation of the proposed method, real-world limitations in measuring the output field would deteriorate the quality of the recovered image. We have found that recovery of the input image was feasible only when using at least 10 bit digitization for the acquired frames, while 8 bit data sampling showed significant reduction in the success rate of image recovery (data not shown). In order to

study the sensitivity of the method to different levels of SNR, random Gaussian noise was numerically added to the simulated camera captures of the transmitted reference and object fields. The recovered images of an input (intensity-only) image of a single cell (Fig. 10, top left panel) are shown for different simulated SNR values (Fig. 10, top panels); data acquisitions with SNRs below 13 dB had resulted in significant reduction of image quality and, occasionally, inability of the algorithm to converge into solutions that resembled the true input fields. Similar results were obtained for the transmission of phase-only image of a single cell (Fig. 10, bottom panels);

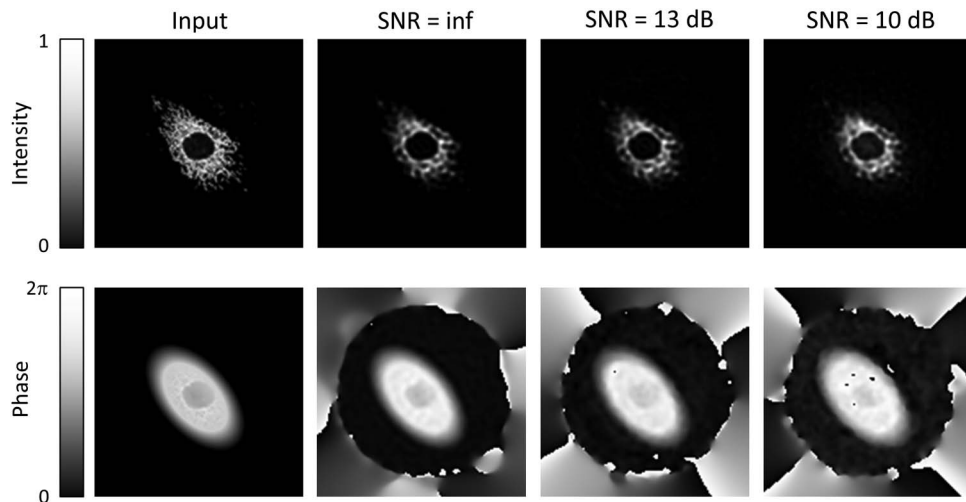


Fig. 10. Simulated transmission of input amplitude-only (top) and phase-only (bottom) fields through a $150\ \mu\text{m}$ core diameter optical fiber ($V = 72.985$) for different SNR levels.

SNRs below 13 dB resulted in limited or no ability to calculate the input field.

7. DISCUSSION

So far, direct image transmission from one end to another of a long multimode fiber has not been demonstrated experimentally. The reason for this difficulty is well known to be the modal dispersion in weakly guiding fibers, which deteriorates the image even after a few millimeters of propagation. In theory, characterizing the modal dispersion of a given fiber could be used for numerically compensating for it; however, long optical fibers are highly sensitive structures and often tend to vary their optical properties even under the slightest external influence. While this property is ideal for sensing the environment [19], it makes image transmission extremely difficult because the fiber's transfer function needs to be constantly monitored.

Our method for overcoming the modal dispersion problem involves the transmission of a reference field in close time proximity to the object image, calculating the fiber's instantaneous modal dispersion, and using the data to calculate the input field. A key challenge in this approach would be the generation and transmission of the reference image: it needs to include at least a portion of all possible propagation modes in order to measure their modal phases and, at the same time, needs to be simple enough to generate experimentally in a repeatable manner. Unfortunately, a single point source, which could be relatively simple to produce, cannot excite all the LP modes. The reference image in this work (Fig. 5) includes all the propagation modes with uniform amplitudes and phases and could still be easily produced in an actual experiment.

Another key aspect for successful image transmission would be the measurement of the output object and reference fields. Our choice to use the simplest possible optical setup for capturing intensity images and to recover the phases using iterative algorithms would be relatively straightforward to implement in the laboratory. Moreover, the large dynamic range and low noise of current CCD and CMOS cameras would potentially allow capturing the transmitted fields with the high accuracy level required for calculating their phases. The total computation time of our modified Gerchberg–Saxton algorithm was only a few seconds and could be further shortened using a dedicated computation system that would permit higher imaging rates.

The number of resolvable points potentially offered by a single multimode fiber would be comparable to the number of fibers (pixels) in a fiber bundle of comparable diameter, albeit using much simpler, longer, and less expensive imaging probes. Obviously, larger-diameter fibers would allow higher-resolution images to be transmitted, at the expense, however, of more sophisticated computation algorithms and longer processing times. Unlike fiber-bundle technology, the single-multimode-fiber approach could also be used to transmit phase images (Fig. 9), which could be useful for imaging biological specimens or for the transmission of three-dimensional complex fields. Color imaging would also be possible with this technique, for example by using three narrowband channels in the blue, green, and red wavelengths.

Compared to the previously published method for image transmission through a multimode fiber [11,12], which uses a spatial light modulator for calculating the fiber's transfer

matrix and transmitting an image comprised of a large number of modes, our approach requires only a single reference field for calibration and could thus be utilized in applications where fast, real-time estimation of the fibers' transfer function is needed, for example in applications that involve occasional fiber motion or operate under varying environmental conditions. In addition, our reference field could, in principle, be generated using a simple amplitude mask and would not necessitate expensive electro-optical components at the transmitting end.

Finally, realizing the proposed technique in the laboratory would face several challenges related mainly to the various simplifying assumptions made during this work. Perhaps the most critical challenge would be associated with the cross talk between the propagation modes; in a preliminary experiment for testing the feasibility of this technique we have observed occasional energy coupling between modes and between different polarizations, which we relate primarily to nonuniformities along the optical fiber. Another difficulty that would need to be addressed is the short time required between the transmissions of the reference and object images; long fibers exposed to motion, strain, or temperature variations would exhibit fast variations in modal dispersion, requiring shorter time periods between field transmissions. It is worth noting, however, that full modal phase computation and input field recovery does not necessarily depend on these time periods; the two fields could be transmitted almost instantaneously using a fast mechanical, electrical, or optical switching, while field computation could be performed at a later time. Still, dedicated computing hardware with a fast processor should be required for any real-time imaging applications.

In conclusion, a novel method for transmitting an image field through a single multimode fiber is theoretically presented and discussed. The method is based on the transmission of a reference field in addition to the image field, which is used for calculating the instantaneous modal dispersion and for recovering the complex input field. Using a relatively simple optical setup, which does not rely on nonlinear optics, fast-moving parts, or interferometry, we expect this method to allow image transmission at high resolutions across long, single optical fibers. Such technology may find important applications in telecommunication, remote sensing, and minimally invasive biomedical imaging.

REFERENCES

1. C. M. Brown, P. G. Reinhall, S. Karasawa, and E. J. Seibel, "Optomechanical design and fabrication of resonant microscanners for a scanning fiber endoscope," *Opt. Eng.* **45**, 043001 (2006).
2. D. L. Dickensheets and G. S. Kino, "Micromachined scanning confocal optical microscope," *Opt. Lett.* **21**, 764–766 (1996).
3. L. Froehly, S. N. Martin, T. Lasser, C. Depeursinge, and F. Lang, "Multiplexed 3D imaging using wavelength encoded spectral interferometry: a proof of principle," *Opt. Commun.* **222**, 127–136 (2003).
4. G. J. Tearney, R. H. Webb, and B. E. Bouma, "Spectrally encoded confocal microscopy," *Opt. Lett.* **23**, 1152–1154 (1998).
5. D. Yelin, I. Rizvi, W. M. White, J. T. Motz, T. Hasan, B. E. Bouma, and G. J. Tearney, "Three-dimensional miniature endoscopy," *Nature* **443**, 765–765 (2006).
6. A. Lucesoli and T. Rozzi, "Image transmission and radiation by truncated linearly polarized multimode fiber," *Appl. Opt.* **46**, 3031–3037 (2007).

7. B. Fischer and S. Sternklar, "Image transmission and interferometry with multimode fibers using self-pumped phase conjugation," *Appl. Phys. Lett.* **46**, 113–114 (1985).
8. G. J. Dunning and R. C. Lind, "Demonstration of image transmission through fibers by optical phase conjugation," *Opt. Lett.* **7**, 558–560 (1982).
9. A. Yariv, "Three-dimensional pictorial transmission in optical fibers," *Appl. Phys. Lett.* **28**, 88–89 (1976).
10. M. Fukui and K.-I. Kitayama, "Real-time restoration method for image transmission in a multimode optical fiber," *Opt. Lett.* **15**, 977–979 (1990).
11. T. Cizmar and K. Dholakia, "Shaping the light transmission through a multimode optical fibre: complex transformation analysis and applications in biophotonics," *Opt. Express* **19**, 18871–18884 (2011).
12. T. Cizmar and K. Dholakia, "Exploiting multimode waveguides for pure fibre-based imaging," *Nat. Commun.* **3**, 1027 (2012).
13. J. A. Bruck, *Fundamentals of Optical Fibers*, 2nd ed. (Wiley, 2004).
14. B. C. Platt and R. Shack, "History and principles of Shack-Hartmann wavefront sensing," *J. Refract. Surg.* **17**, S573–S577 (2001).
15. C. Bamber, B. Sutherland, A. Patel, C. Stewart, and J. S. Lundeen, "Measurement of the transverse electric field profile of light by a self-referencing method with direct phase determination," *Opt. Express* **20**, 2034–2044 (2012).
16. S. A. Eastwood, A. I. Bishop, T. C. Petersen, D. M. Paganin, and M. J. Morgan, "Phase measurement using an optical vortex lattice produced with a three-beam interferometer," *Opt. Express* **20**, 13947–13957 (2012).
17. C. Falldorf, M. Agour, C. V. Kopylov, and R. B. Bergmann, "Phase retrieval by means of a spatial light modulator in the Fourier domain of an imaging system," *Appl. Opt.* **49**, 1826–1830 (2010).
18. R. W. Gerchberg and W. Saxton, "A practical algorithm for the determination of the phase from image and diffraction plane pictures," *Optik* **35**, 237–246 (1972).
19. B. Lee, "Review of the present status of optical fiber sensors," *Opt. Fiber Technol.* **9**, 57–79 (2003).